Polymer 239 (2022) 124435

Contents lists available at ScienceDirect

Polymer

journal homepage: www.elsevier.com/locate/polymer

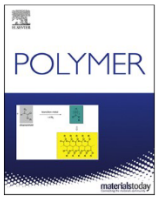

Integrated analysis of chain orientation induced anisotropy in nanoimprinted PVDF based copolymers

Wen Qian [a,1], Shuo Sun [b,1], Tyler J. Johnson [c], Charles Nguyen [a], Stephen Ducharme [b,**], Joseph A. Turner [a,*]

[a] Department of Mechanical and Materials Engineering, University of Nebraska-Lincoln, Lincoln, NE, 68588-0526, USA
[b] Department of Physics and Astronomy and Nebraska Center for Materials and Nanoscience, University of Nebraska-Lincoln, Lincoln, NE, 68588-0299, USA
[c] Department of Chemical and Biomolecular Engineering, University of Nebraska-Lincoln, Lincoln, NE, 68588-0643, USA

ARTICLE INFO

Keywords:
PVDF
Chain orientation
Anisotropy
Localized molecular vibration
Localized mechanical property

ABSTRACT

Poly(vinylidene fluoride) (PVDF) and its copolymers are electrically active materials that have the ability to harvest mechanical energy through mechanical vibrations and structural flexing. Due to the inherent nanoscale dependency of the molecular structure of PVDF copolymer, efficient methods for investigating the effects of chain orientation on its localized nanomechanical properties are very limited. In this manuscript, we use infrared atomic force microscope (IR-AFM), contact-resonance atomic force microscopy (CR-AFM), scanning electron microscopy (SEM), and high resolution transmission electron microscopy (TEM), to reveal the correlations between localized molecular vibration, anisotropy, and the corresponding dynamic nanomechanical properties. IR-AFM is able to probe the chain orientation of the PVDF copolymer and CR-AFM is able to resolve the in-plane anisotropy along the axis of the polymer chain. The combination of these techniques can provide a quick, effective, nondestructive method to reveal the formation mechanisms, which could lead to optimization of the electroactive polymer organization.

1. Introduction

Poly (vinylidene fluoride) (PVDF), a well-recognized electroactive polymer, has been studied extensively in the past [1]. Discovery of the switchable ferroelectric polarization in ultrathin films of copolymers of PVDF with trifluoroethylene P(VDF-TrFE) has generated great interest for applications in organic electronics, biocompatible tissue engineering, and memory devices [2,3]. Such electroactive polymers derive their macroscale electromechanical response from the material organization at the atomic, nano-, and micro-scales. However, current material design does not fully exploit the opportunity to enhance macroscale performance through optimization of the polymer organization because of the limited availability of quantitative methods to quantify nanoscale mechanical properties. For ferroelectric P(VDF-TrFE) copolymers, the influence of the nanoscale structure on mechanical response is still not well understood.

Recently, we have discovered that the electromechanical response of P(VDF-TrFE) copolymers can be greatly enhanced with applied forces that affect the nanoscale organization [4–7]. This result is enabled by the deep understanding that has accumulated in recent years into the mechanisms and kinetics of self-assembly of plastic crystals at the nanoscale [8–10]. Recent literature reported how nanostructure manipulation, from nanoimprinting and induced self-assembly ensembles, can enhance the piezoelectric properties found in electroactive polymers [11,12]. Lee et al. showed the effect of nanoconfinement on preferential orientation and crystallization with reduced structural defects [13], which can result in an increase of the piezoelectric coefficient d_{33}, exceeding the values d_{31} and d_{32} by 30% and greater [14,15]. This anisotropy in the crystal structure is related to the mechanical properties. Efforts to control the mechanical properties of P(VDF-TrFE) copolymers are needed, but investigations to do so require a better understanding of the molecular structure, chain orientation, in-plane anisotropy mechanisms and kinetics for piezoelectric polymers, which can be influenced by the nanostructure in the film [16,17].

* Corresponding author.
** Corresponding author.
E-mail addresses: sducharme@unl.edu (S. Ducharme), jaturner@unl.edu (J.A. Turner).
[1] These authors contributed equally to this work.

https://doi.org/10.1016/j.polymer.2021.124435
Received 21 August 2021; Received in revised form 13 November 2021; Accepted 4 December 2021
Available online 8 December 2021
0032-3861/

The infrared atomic force microscope (IR-AFM) is a rapidly emerging instrument that provides chemical analysis and compositional mapping with spatial resolution that is far beyond conventional optical diffraction limits [18,19]. IR-AFM works by using the tip of an AFM contact probe to detect the local thermal expansion in a sample resulting from absorption of infrared radiation. Therefore, it can provide nanoscale spatial resolution, which is effectively limited only by the AFM tip contact area [20,21]. Recently, the IR-AFM has been shown to be a unique, high-sensitivity instrument to study the molecular orientation of polymers through polarized IR laser in order to induce a signal enhancement from the bands oriented along the polarization direction [22,23]. Therefore, it is ideally suited to study the molecular orientation of P(VDF-TrFE) copolymer via probing both in-plane and out-of-plane vibration components.

The contact-resonance atomic force microscopy (CR-AFM) technique is a dynamic contact mode based on the determination of the resonance frequencies and quality factors Q_n of an AFM cantilever in free space and in contact with a sample surface [24,25]. The mechanical properties are calculated from the measured f_n and Q_n via analytical representations of the cantilever dynamics and tip-sample contact mechanics [25]. Recently this technique has been extended to quantify viscoelastic property measurements, such as storage modulus, loss modulus, and loss tangent at the nanoscale [26,27]. The vertical (out-of-plane) and lateral (in-plane) spectrum can be recorded simultaneously to reveal the distribution of the polymer chain axis, the polar anisotropy and azimuthal variations in the signal of the lateral vibration modes which can be attributed to the local in-plane stiffness [28].

In this article, we report the use of complementary nanoscale characterization techniques by integrating IR-AFM, CR-AFM, high resolution transmission electron microscopy (TEM), and scanning electron microscopy (SEM) to investigate the localized morphology, crystalline structure, chain orientation, in-plane anisotropy, Young's modulus E, and shear modulus G of a ferroelectric P(VDF-TrFE) copolymer. The experimental demonstration of anisotropy within nanostructures will provide new insight into the polymer organization. We believe this approach would eventually aid in the understanding of formation mechanisms to regulate the size, morphology, and distribution of nanostructures, and to achieve high crystallinity and orientation with optimized mechanical properties. To the best of our knowledge, the localized mechanical properties and in-plane anisotropy for PVDF based copolymers have not been examined previously.

2. Experimental section

2.1. PVDF thin film and nanostructures preparation

The P(VDF-TrFE) (70:30 mol%) ferroelectric polymer powder, purchased from Solvene 250, was first dissolved in methyl ethyl ketone (MEK) with a concentration of 3 wt%. Then, the P(VDF-TrFE) films were prepared by spin coating on top of a SiO_2/Si substrate at 2000 rpm. After that, the P(VDF-TrFE) films were annealed at 135 °C for 1 h for the purpose of improving their crystallinity. For TEM analysis, samples were prepared by dissolving the P(VDF-TrFE) ferroelectric polymer powder in MEK as described above, then dispersed the solution on Lacey carbon/thin film copper grid (400 Mesh), then finally annealed at 135 °C for 1 h.

Nanoimprint lithography was carried out with a SPECAC hydraulic press system. First, the polydimethylsiloxane (PDMS) soft-mold was prepared from a blue-ray DVD disc. The pattern of the PDMS mold was about 300 nm in width, 100 nm in height, and had a period of 600 nm in a rectangular array. Then, the same P(VDF-TrFE) powder was dissolved in dimethylsulfoxide with a concentration of 5 wt%. Next, 5 monolayers of thin film were deposited on a Si substrate by using the horizontal Langmuir-Blodgett (LB) method. Next, the PDMS mold was placed face-down on the polymer-coated substrate, with a pressure ranging from 2.6 bar to 3.0 bar, and heated to 135 °C for 1 h. The sample was then cooled down to room temperature for 90 min and the mold was separated after the pressure was released.

2.2. Morphology, structural and mechanical property measurement

The morphology and chain orientation of PVDF copolymer thin films were observed using a field-emission scanning electron microscope (FESEM, FEI Helios Nanolab 660), and an atomic force microscope (Asylum 3D MFP bio AFM). TEM analysis data was performed on an FEI TECNAI Osiris TEM operated at 200 kV with an attached Gatan Imaging Filter (GIF). The largest condenser aperture (150 μm) and objective aperture were selected for low energy loss measurements. All images and spectra were processed with Gatan's Digital Micrograph software package and were recorded using a GIF CCD camera at a resolution of 512x512 pixels. The energy-filtered images utilize a broad electron beam and parallel acquisition, offering rapid data accumulation on the order of minutes or less. The intrinsic lattice structure of the PVDF copolymer was examined at an accelerating voltage of 200 kV and confirmed that single grains include well-crystallized regions and partially crystallized regions. In order to obtain the best signal-to-noise ratio, some additional optimization steps were achieved by adjusting the window width and position with respect to the energy-loss. X-ray diffraction (XRD) pattern measurements for phase identification were performed in the 2θ range of 10°–30° using a Rigaku Ultima IV XRD system with graphite monochromatized Cu Kα radiation (λ = 1.54187 Å). The localized mechanical properties (elastic modulus) at the nanoscale were measured with an atomic force microscope (AFM) by performing quasi-static force-displacement curves on the sample surface. For comparison with the mechanical properties at the microscale, a series of quasi-static nanoindentation measurements for the bulk film were performed using a Hysitron TI 950 Triboindenter.

2.3. Localized nanoIR spectrum and chemical mapping

A commercial nano-IR2 atomic force microscope (Anasys Instruments, Inc.) supplemented with a tunable infrared quantum cascade laser, QCL (Daylight Solutions MIRcat), was used to measure both topography images and localized nano-IR spectra, as well as to create chemical IR maps at a constant wavenumber. Contact mode nIR2 probes (Model: PR-EX-nIR2, Anasys Instruments) with resonance frequency of 13 ± 4 kHz and spring constant of 0.07–0.4 N/m were used. The AFM-IR technique was accomplished by coupling a pulsed tunable IR source with an AFM, which has a pulse length of ~10 ns and can cover a broad range of the mid-IR region. The light from the IR laser was focused onto the surface region near the tip-sample contact area. When the sample absorbed the light, a rapid heating/expansion of the sample occurred, creating an impulsive load onto the AFM cantilever tip, which induced an oscillation. The amplitude of cantilever oscillation was proportional to the sample IR absorption coefficient. Spectra were acquired with two perpendicular directions of infrared laser light. Vector normalization was applied to all spectra in order to visualize and compare spectral shape/peak ratios of spectrum.

2.4. CR-AFM measurement

All CR-AFM spectra were recorded on the Anasys afm+ (Anasys Instruments, Santa Barbara, CA) with a Thermalever™ probe model AN2-300, which has a first free vibrational resonance frequency in the range of 20–35 kHz and spring constant k_c ~0.35 N/m. The measured free-space resonance frequencies were respectively 23.5 kHz and 151.6 kHz for the first and the second bending modes. The contact-resonance spectra were measured in the frequency ranges 110–120 kHz (first mode) and 350–400 kHz (second mode). Taking into account that the tip-sample contact stiffness increased with the applied static load, we assumed a spherical tip geometry (n = 3/2). In each set of experiments, a reference measurement was performed both before and after each measurement on a thin-film sample. Such a procedure allowed us to

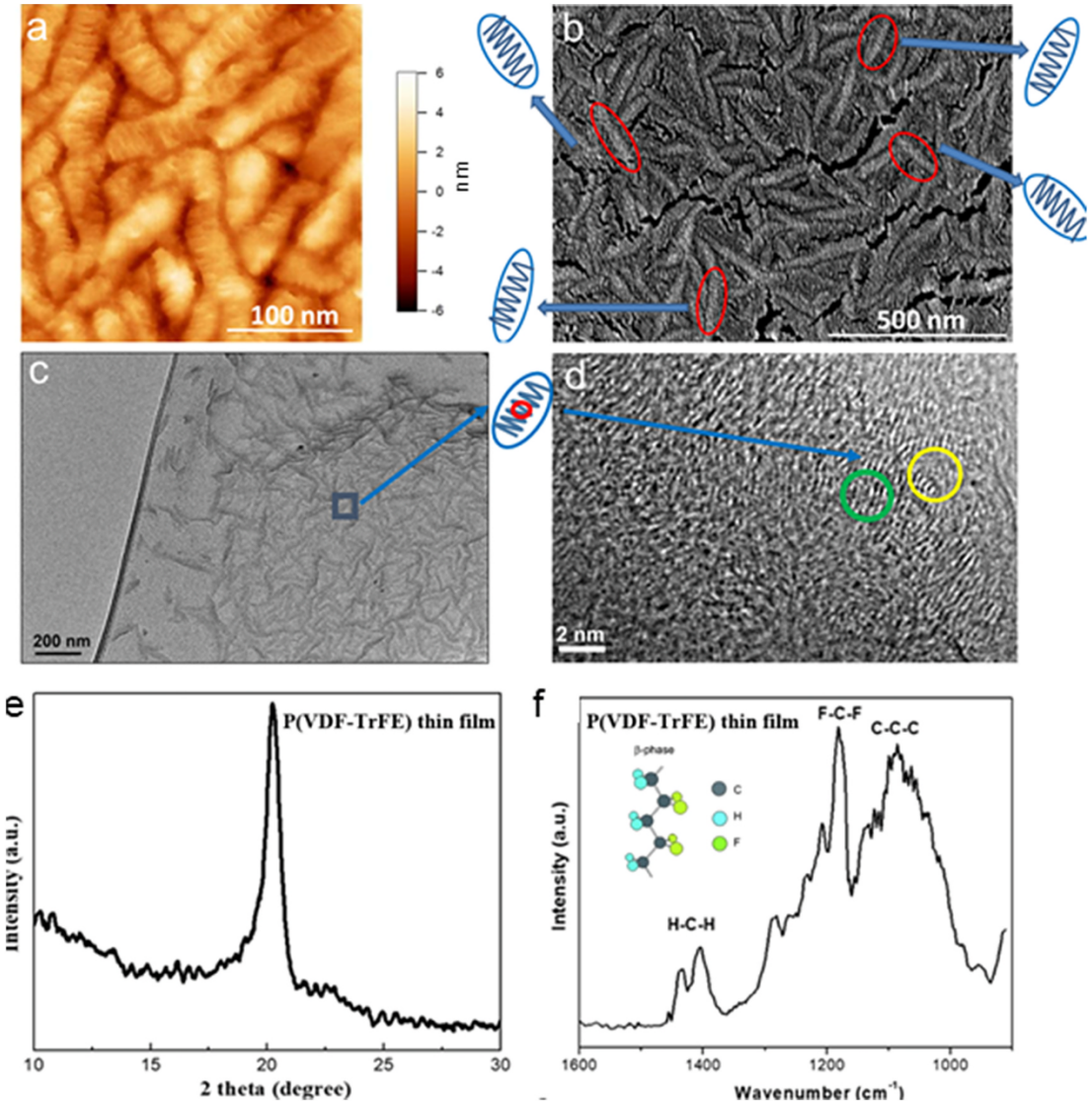

Fig. 1. (a) High resolution AFM topography image of PVDF copolymer thin film with a scan area of 270 nm × 270 nm; (b) High resolution SEM image showing the orientation of polymer chain; (c) Low magnification TEM image; (d) High magnification TEM image showing the crystalline structure within one grain; (e) XRD pattern from PVDF copolymer thin film; (f) Localized nanoscale IR spectra on a single rice grain.

account for tip wear. The probe tip radius was approximately 35 nm. The static load force applied in experiments varied from 20 nN to 100 nN. Therefore, the influence of the substrate on the measured elastic properties of the film can be estimated by a comparison of the deformations occurring at the film surface and film–substrate interface. The drive amplitude was set as low as possible to ensure linear tip-sample contact. For PVDF copolymer nanostripes, the amplitude ranged from 0.50–2.10 for the 1st symmetric mode and 0.15–0.60 for the lateral mode; For polycarbonate, the amplitude varied from 0.90–1.20 for the 1st symmetric mode and 0.30–0.35 for the lateral mode.

3. Results and discussion

Fig. 1a shows an AFM topography image of a PVDF copolymer thin film with a scan area of 270 nm × 270 nm. Fig. 1b shows an SEM image of the typical "rice-grain" morphology of the PVDF copolymer thin films. Both the AFM and SEM images are consistent, clearly showing that polymer chains have specific orientations after the fine annealing process [9]. The dimension of each rice grain is around 100–200 nm. Due to the limited resolution of 5 nm–10 nm for SEM and AFM, we acquired high-magnification TEM images to probe the crystalline structure within a single "rice grain" (Fig. 1c–d). Fig. 1d confirms that single grains include well-crystallized regions (indicated by the green circle) and partially crystallized regions (indicated by the yellow circle). Comprehensive analysis of the high resolution AFM, SEM, and TEM images allowed us to investigate the statistics of the chain orientation, crystalline structure and crystalline degree, which would enable us to optimize the processing methods eventually to improve the polymer chain organization. To confirm that this bulk film is in the polar electroactive β-phase, XRD analysis was performed (Fig. 1e). The reflection peak of 2θ at 19.7° corresponded well with the (110) and (200) diffraction peaks of the β-phase crystal structure [11]. The crystallinity degree can be calculated by dividing the total area of crystalline peaks by the total area under the diffraction curve (crystalline plus amorphous peaks). The crystallinity degree improved up to 55% in comparison with a non-annealed spun film [29–31]. Positioning the AFM probe tip to a specific location, we could acquire the localized IR spectrum with nanoscale resolution. The probe tip radius was approximately 50 nm, which was far below the conventional optical diffraction limit [32]. As shown in Fig. 1f, the C-C antisymmetric stretching, CF_2 antisymmetric stretching, CH_2 wagging and CH_2 bending stretch of all-trans (TT) chains structure at 1076 cm^{-1}, 1184 cm^{-1}, 1401 cm^{-1} and 1432 cm^{-1}, are the

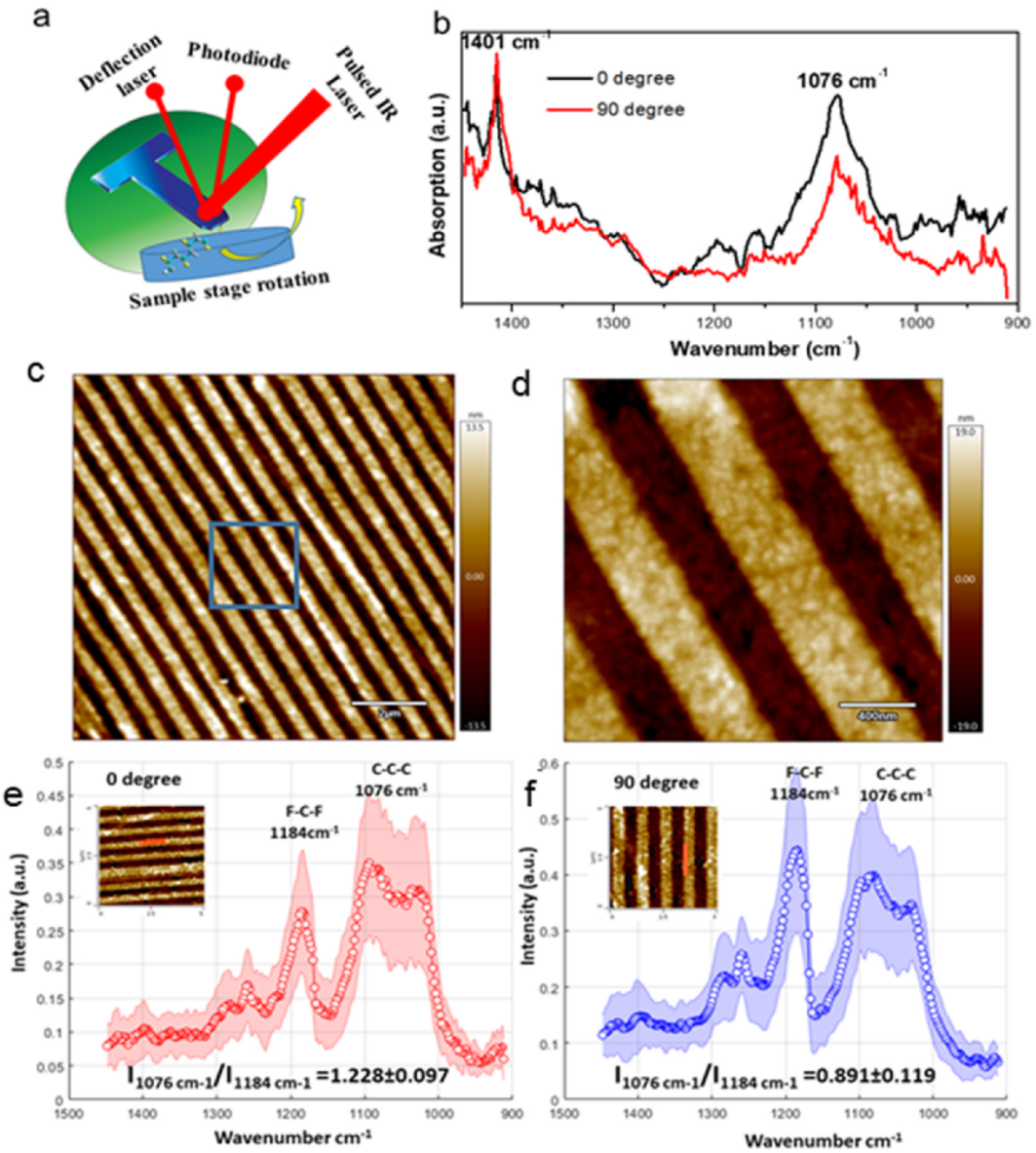

Fig. 2. (a) Schematic illustration of molecular vibration under different irradiated IR laser direction; (b) Localized nanoIR spectrum comparison between 0° and 90° of laser direction; (c) AFM topography image of PVDF nanostripes in the scan area of 10 × 10 μm^2; (d) enlarged area of 2 × 2 μm^2; (e–f) Array of localized IR spectrum of PVDF nanostripes comparison between 0° and 90° of laser direction.

fingerprint for the β-phase in the IR spectrum [33,34]. A small shift in the wavenumbers of peak position was found due to instrument variation.

The nanoIR technique was used to identify the molecular orientation of individual "rice grains" as revealed by the investigation of associated changes of localized nanoIR spectra when the input IR laser direction was changed. The vibration direction of C-C anti symmetric stretching (1076 cm^{-1}) was aligned with the C-C body chain. If the vibration direction is parallel to the IR laser direction, the IR absorption will be greatly enhanced. On the contrary, if the vibration direction is perpendicular to the laser direction, the IR absorption will be limited [35,36]. In order to investigate the chain orientation, we changed the direction of the IR laser by rotating the sample stage from 0° to 90° (Fig. 2a). The localized spectrum shows a difference of peak intensity ratio of 1076 cm^{-1}/1401 cm^{-1}, which is relatively high for 0° compared with 90° (Fig. 2b). This result indicated that the C-C antisymmetric stretching vibration at 1076 cm^{-1} was very sensitive to irradiation direction. Fig. 2c–d shows the AFM topography images of the nanoimprinted PVDF copolymer nanostripes in a scan area of 10 × 10 μm^2 (c) and an enlarged area of 2 × 2 μm^2 (d), respectively. We recorded the localized IR spectra at 0° and 90° on the same nanostripe using a total of 14 measurement positions. Fig. 2e–f shows the averaged spectra with shaded error bar which exhibit the same band profile but with different peak intensity ratios for the 0° and 90° orientations, respectively. For 0°, the peak intensity ratio of 1076 cm^{-1}/1184 cm^{-1} is 1.228 ± 0.097; For 90°, the peak intensity ratio of 1076 cm^{-1}/1184 cm^{-1} is lower (0.891 ± 0.119). The details of peak intensity for each spectrum are shown in Table S1 (supplementary information). Absorption bands of specific functional groups become weaker which is related to the orientation of the group towards the direction of the laser electromagnetic field. Thus, we hypothesize that hydrocarbon chains are oriented perpendicular to the substrate and thereby relatively parallel to the applied infrared laser direction.

We also performed chemical IR mapping at a fixed wavenumber of 1076 cm^{-1}, using the same scan area (Fig. 3). One topography image (Fig. 3a) was recorded with the laser direction at 90° and the other topography image (Fig. 3c) was recorded with the laser direction at 5°. The height profile for the images is nearly the same, but the chemical IR

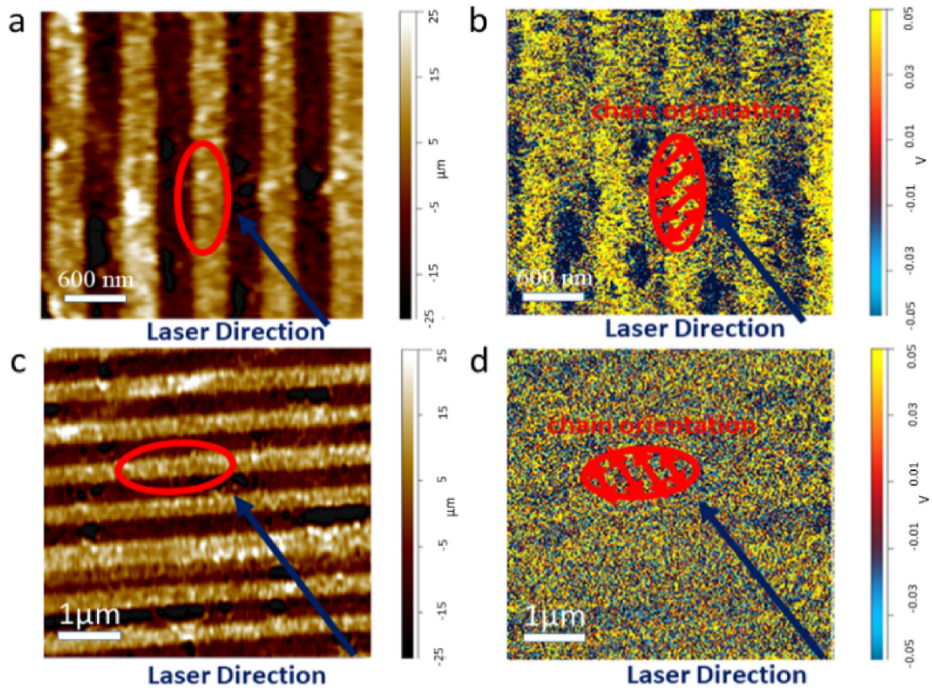

Fig. 3. AFM topography images of PVDF nanostripes and the corresponding IR mappings at 1076 cm^{-1} comparison between 90° (a–b) and 5° of laser direction (c–d).

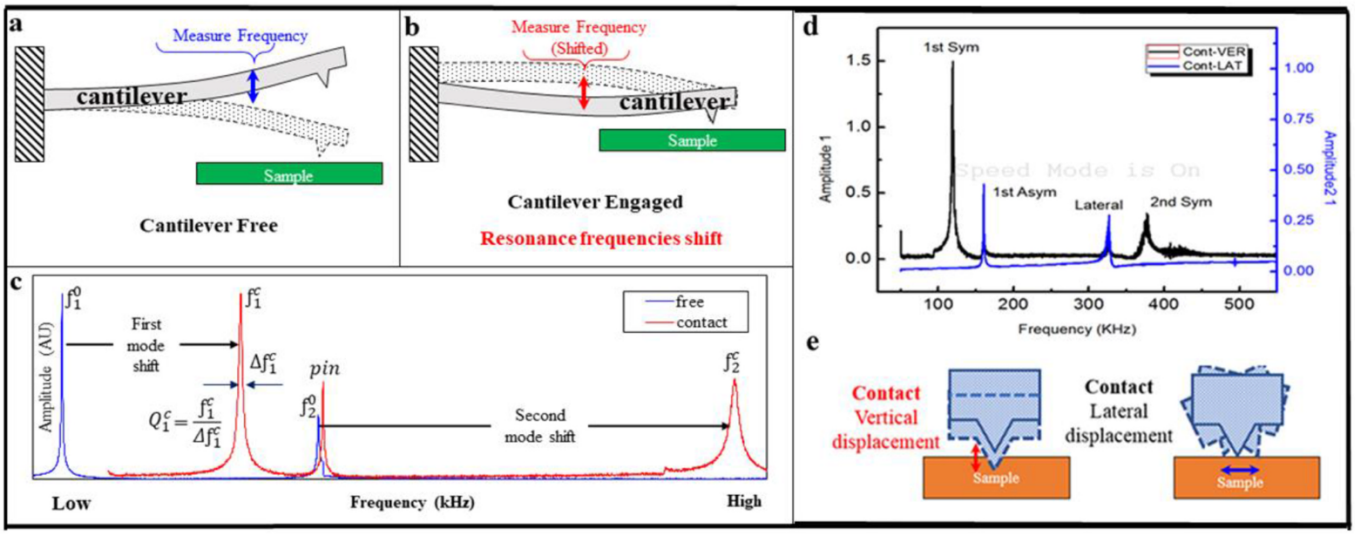

Fig. 4. Schematics of the CR-AFM cantilever vibration in the lowest-frequency free mode (a) and lowest-frequency contact mode (b). (c) Contact-resonance spectra from the free mode and contact mode. (d) Contact-resonance spectrum from both vertical and lateral channels in contact mode, (e) Illustration of the two-dimensional model for motions at vertical and lateral displacement, respectively.

map is different. We noticed that in the circled highlighted area, while the direction angle was 90°, the IR absorption intensity was much stronger (Fig. 3b); for the direction angle of 5°, the IR absorption intensity was relatively low (Fig. 3d). A random orientation would imply no contrast changes, therefore, comparison between these two IR mappings clearly indicates that the polymer chain has a specific orientation, and we can infer the chain orientation of specific "rice grains" based on the IR laser direction. The mapping contrast difference is based on the number of C-C chains that can be excited, whether the alignment of the molecular vibration is aligned with the IR laser direction or not. It is clear that nanoIR chemical mapping can provide a unique, quick, effective, and nondestructive method to study polymer chain orientation with nanoscale resolution.

The CR-AFM measurements were performed using the Anasys afm+ with a U-shaped cantilever, which can be excited vibrationally using the Lorentz force. When a magnetic field is applied to the cantilever, a Lorentz force is generated, which is perpendicular in direction to both current and applied magnetic field. When an AC voltage is applied, a force will be generated in two directions leading to oscillations of cantilever at given amplitude allowing probing of the sample. Because there are no moving parts actuating the cantilever, Lorentz contact resonance provides a very clean excitation over broad frequency ranges [37]. The U-shape cantilever was first oscillated above the test sample while out of contact, commonly referred to as the free case (Fig. 4a). The cantilever was then engaged with the sample of interest, and the frequency spectrum of the response was recorded (Fig. 4b). The photodiode

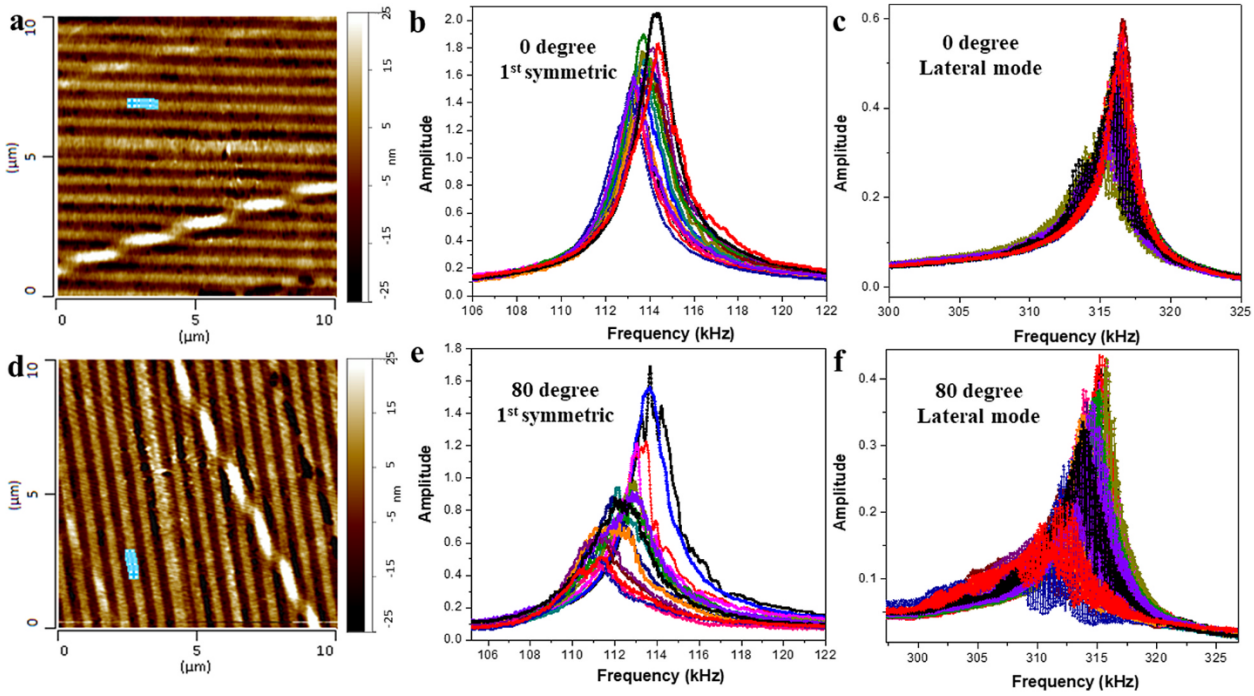

Fig. 5. (a–c) AFM topography image (a), and contact resonance spectrum of PVDF nanostripes at sample stage of 0° for the 1st symmetric resonance (b), and for the lateral resonance (c); (d–f) AFM topography image (d), and contact resonance spectrum of PVDF nanostripes at sample stage of 80° for the 1st symmetric resonance (e), and for the lateral resonance (f).

detector on the AFM can measure both the vertical and lateral deflection of the laser, allowing for out-of-plane and in-plane vibration measurements simultaneously. When the AFM tip was in contact with sample surface, the resonances shifted from their free mode to their contact mode as shown in Fig. 6c. The relative shift of each resonance frequency was used to determine an equivalent contact stiffness and damping between the AFM tip and the sample. The CR-AFM spectra were obtained from a free case and a contact case to obtain frequency spectra f_n^0 and f_n^C, quality factors Q_n^0 and Q_n^C, for the nth flexural eigenmode respectively, which were then used to determine viscoelastic properties of storage modulus E' and loss modulus E''. The flexural spring constant of the cantilever is $k_{\text{lever}} = Eb^3w/4{L_1}^3$, where E is Young's modulus. The lateral stiffness is $S_{\text{lever}} = wb^3G/3Lh^2$, where G is the shear modulus. More details of cantilever dimensions are presented in the

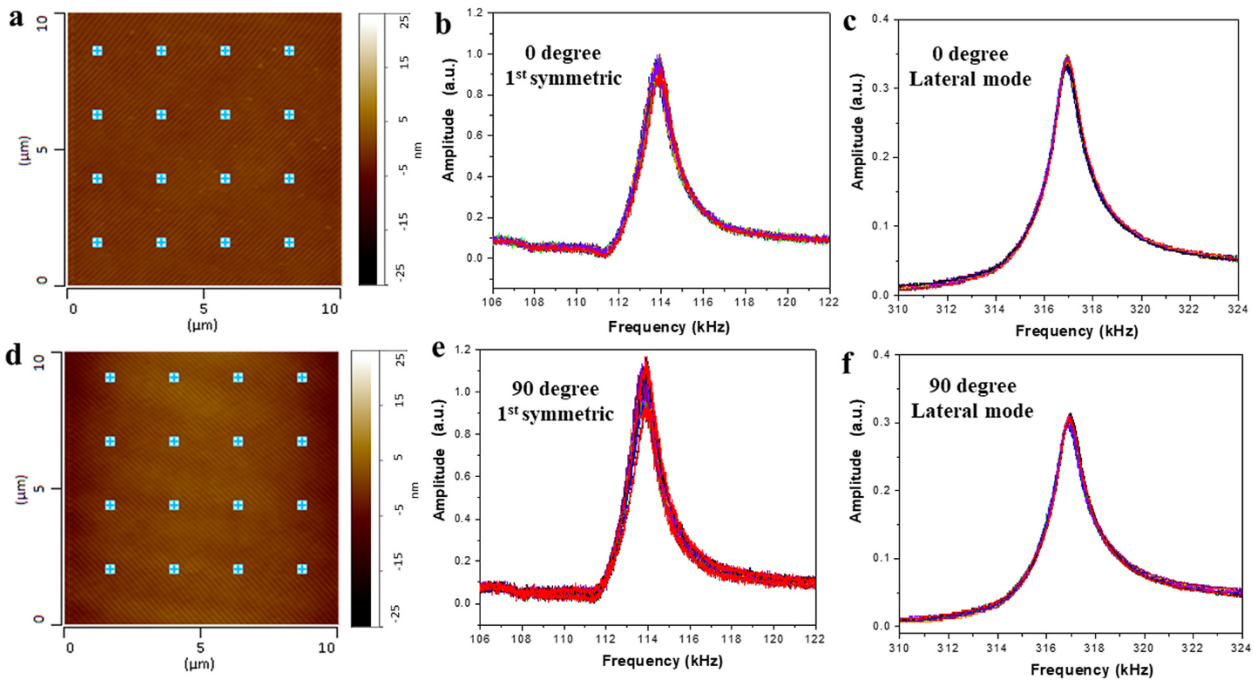

Fig. 6. (a–c) AFM topography image (a), and contact resonance spectrum of isotropic polycarbonate at sample stage of 0° for the 1st symmetric resonance (b), and for the lateral resonance (c); (d–f) AFM topography image (d), and contact resonance spectrum of isotropic polycarbonate at sample stage of 80° for the 1st symmetric resonance (e), and for lateral resonance (f).

supplementary information (Figs. S1 and S2). Fig. 4d–e shows the CR-AFM spectra from the PVDF copolymer thin film sample for both vertical (d) and lateral (e) response of flexural modes. The peaks labelled "1st Sym" and "Lateral" correspond to the out-of-plane and in-plane relationship between the two cantilever legs, and therefore the vertical and lateral responses, respectively, of the sample [38,39]. We identified the first symmetric mode (out-of-plane) at ~123 kHz and the lateral mode (in-plane) at ~316 kHz for the contact vibration case. We recorded the contact resonance spectrum with different values of the applied force (setpoint) ranging from 0.5 V to 2.0 V. The anisotropic mechanical response of the sample can be derived from the amplitudes and *Q* factors of the lateral mode resonance peaks. More details of contact resonance theory and the mechanical model are presented in the supplementary information.

Each CR-AFM spectrum is inherently related to the in-plane anisotropic properties of the sample [39]. The orientation of the PVDF copolymer molecular structure dependency can be investigated by rotation of the sample stage. To demonstrate this capability, we selected the confined PVDF copolymer nanostripes as the test sample, because they had one-dimensional molecular chains that were hundreds of micrometers in length [8]. During the contact resonance spectrum measurement, all parameters were the same, but the sample stage was rotated from 0 to 80°. Fig. 5a shows the AFM height images of PVDF copolymer nanostripes at 0°. Fig. 5b shows the first symmetric resonance peak which was in the range of 113.1–114.3 kHz at 0° for a total of 16 positions. Fig. 5c shows the lateral resonance peak range from 314.7 kHz to 317.2 kHz at 0° for a total of 14 spectra. Then the sample stage was rotated to 80°, and the AFM topography imaged and contact resonance spectra were recorded again on the same nanostripe, as shown in Fig. 5d–f. Comparison of Fig. 5b with Fig. 5e (peak range from 111.7 kHz to 114.6 kHz), shows a resonance frequency shift of 1.4 kHz for the first symmetric mode. Comparison of Fig. 5c with Fig. 5f (peak range from 312.1 kHz to 315.9 kHz), shows a resonance frequency shift of 2.6 kHz for the lateral mode. Ideally, for the first symmetric mode, the tip would move nearly parallel to the polymer chain, and for the lateral mode, the lateral tip oscillation direction would be perpendicular to the polymer chain structures. The distribution of the polymer chain axes is attributed to the local stiffness of the in-plane anisotropy. The variance existing in both the first symmetric mode and the lateral mode is due to the contact resonance AFM probe approaching the sample surface of anisotropy PVDF copolymer with a tilted angle of 12–15°. We also measured the contact resonance spectrum on an isotropic polycarbonate bulk film using the same method (Fig. 6a–f), which showed no resonance frequency shift for both the first symmetric mode and the lateral mode. The results clearly demonstrate that CR-AFM can aid in the understanding of formation mechanisms, to optimize the electroactive anisotropy organization, to achieve high crystallinity with good mechanical properties.

In the lateral mode analysis, the lateral spring and dashpot in the model act to quantify deformations parallel to the plane of the sample (i.e., the shear modulus and damping). The adapted lateral model does not account for lateral and vertical coupling (i.e., springs and dashpots in both vertical and lateral directions for tip-sample contact), but rather is restricted to the corresponding motion (lateral vibration and tip-sample shearing interaction) separately. Additionally, we used an effective tip position ($\gamma \cong 0.94$) that was calculated for the mode crossing of the 1st and 2nd vertical flexural modes when calculating the lateral mode stiffness and damping [40].

An in-house program to analyze the frequency response of CR-AFM data, intelligent contact resonance AFM for viscoelasticity (iCRAVE) [41], was developed to evaluate the frequency response of the mechanical system. Using iCRAVE, the storage modulus, loss modulus and loss tangent values were extracted from a model fit of the 1st vertical resonance. We chose a 2.0 μm thick bulk film as the calibration sample for the iCRAVE calculations. The quasi-static nanoindentation result (Fig. S3), the storage/loss modulus and shear storage/loss modulus values of bulk film are included in Supplementary Information. Using iCRAVE, the quantitative values of storage modulus, loss modulus and loss tangent of PVDF copolymer nanostripes and polycarbonate at 0° and 90° are shown in Table 1. The quantitative values of shear storage modulus, shear loss modulus and shear loss tangent values were determined from a model fit of the lateral resonance, which are shown in Table 2.

Table 1
Comparison of storage modulus, loss modulus and loss tangent of PVDF copolymer nanostripes and polycarbonate at 0° and 90°.

Sample	Storage Modulus (GPa)		Loss Modulus (GPa)		Loss Tangent	
	0°	90°	0°	90°	0°	90°
PVDF nanostripes	3.324 ± 1.028	5.536 ± 1.001	0.099 ± 0.048	0.120 ± 0.057	0.031 ± 0.015	0.021 ± 0.006
Polycarbonate	5.732 ± 0.142	5.548 ± 0.118	0.040 ± 0.002	0.041 ± 0.002	0.007 ± 0.000	0.007 ± 0.000

Table 2
Comparison of shear storage modulus, shear loss modulus and shear loss tangent of PVDF copolymer nanostripes and polycarbonate at 0° and 90°.

Sample	Shear Storage Modulus (GPa)		Shear Loss Modulus (GPa)		Shear Loss Tangent	
	0°	90°	0°	90°	0°	90°
PVDF nanostripes	2.355 ± 0.272	2.940 ± 0.182	0.076 ± 0.026	0.039 ± 0.015	0.033 ± 0.014	0.013 ± 0.005
Polycarbonate	4.010 ± 0.036	3.955 ± 0.031	0.015 ± 0.000	0.017 ± 0.000	0.004 ± 0.000	0.004 ± 0.000

4. Conclusions

Using complementary techniques of infrared atomic force microscope, contact resonance atomic force microscope, transmission electron microscope, scanning electron microscope, and nanoindentation, the correlations between localized molecular vibration, crystalline structure, chain orientation and nano-mechanical properties for PVDF copolymer have been revealed. IR-AFM and chemical mapping provide a quick, effective, nondestructive method for investigating the chain orientation of PVDF copolymers by changing the IR laser direction. CR-AFM can quantify the localized viscoelastic properties of PVDF copolymer nanostructures, determine Young's modulus *E* and shear modulus *G* simultaneously, and more importantly allow investigation of the chains orientation induced anisotropy within individual grains. The comprehensive analysis will enable us to optimize the electroactive polymer organization, to guide improvements in the fabrication process, and finally to achieve high-performance, environmentally-benign, flexible, energy-harvesting devices.

Data availability

The raw/processed data required to reproduce these findings cannot be shared at this time as the data also forms part of an ongoing study.

CRediT author statement

W.Q. and S.S. contributed equally to this work. J.T. and S.D. supervised the project. W.Q. carried out SEM, TEM analysis. S.S. prepared the P(VDF-TrFE) samples and performed XRD measurement. W.Q. and S.S. performed the CR-AFM and IR-AFM measurement. T.J. and C.N. performed the contact resonance modelling. W.Q. and J.T. wrote the

manuscript, and all authors reviewed the manuscript.

Declaration of competing interest

The authors declare that they have no known competing financial interests or personal relationships that could have appeared to influence the work reported in this paper.

Acknowledgements

We thank Dr. Jingfeng Song for the help in acquiring the AFM image of Fig. 1a. Manufacturing and characterization analysis were performed at the NanoEngineering Research Core Facility (NERCF), which is partially funded by the Nebraska Research Initiative. This work was supported by the Nebraska Center for Energy Sciences Research and by the Nebraska Research Initiative.

Appendix A. Supplementary data

Supplementary data to this article can be found online at https://doi.org/10.1016/j.polymer.2021.124435.

References

[1] P. Martins, A.C. Lopes, S. Lanceros-Mendez, Electroactive phases of poly (vinylidene fluoride): determination, processing and applications, Prog. Polym. Sci. 39 (4) (2014) 683–706.
[2] L.M. Blinov, V.M. Fridkin, S.P. Palto, A.V. Bune, P.A. Dowben, S. Ducharme, Two-dimensional ferroelectrics, Usp. Fiz. Nauk 170 (3) (2000) 247–262.
[3] X. Chen, X. Han, Q.D. Shen, PVDF-based ferroelectric polymers in modern flexible electronics, Adv. Electron. Mater. 3 (5) (2017).
[4] B.J. Rodriguez, S. Jesse, S.V. Kalinin, J. Kim, S. Ducharme, V.M. Fridkin, Nanoscale polarization manipulation and imaging of ferroelectric Langmuir-Blodgett polymer films, Appl. Phys. Lett. 90 (12) (2007).
[5] S. Poddar, K. Foreman, S. Adenwalla, S. Ducharme, Finite-size scaling of flexoelectricity in Langmuir-Blodgett polymer thin films, Appl. Phys. Lett. 108 (1) (2016).
[6] Z. Hu, M. Tian, B. Nysten, A.M. Jonas, Regular arrays of highly ordered ferroelectric polymer nanostructures for non-volatile low-voltage memories, Nat. Mater. 8 (1) (2009) 62–67.
[7] Y.-Y. Choi, P. Sharma, C. Phatak, D.J. Gosztola, Y. Liu, J. Lee, B. Lee, J. Li, A. Gruverman, S. Ducharme, S. Hong, Enhancement of local piezoresponse in polymer ferroelectrics via nanoscale control of microstructure, ACS Nano 9 (2) (2015) 1809–1819.
[8] J.Y. Li, Y. Luo, M.J. Bai, S. Ducharme, Nanomesa and nanowell formation in Langmuir-Blodgett polyvinylidene fluoride trifluoroethylene copolymer films, Appl. Phys. Lett. 87 (21) (2005).
[9] M.J. Bai, M. Poulsen, S. Ducharme, Effects of annealing conditions on ferroelectric nanomesa self-assembly, J. Phys.-Condes. Matter 18 (31) (2006) 7383–7392.
[10] M.J. Bai, S. Ducharme, Ferroelectric nanomesa formation from polymer Langmuir-Blodgett films, Appl. Phys. Lett. 85 (16) (2004) 3528–3530.
[11] J.F. Song, H.D. Lu, S.M. Li, L. Tan, A. Gruverman, S. Ducharme, Fabrication of ferroelectric polymer nanostructures on flexible substrates by soft-mold reverse nanoimprint lithography, Nanotechnology 27 (1) (2016).
[12] J.F. Song, H.D. Lu, K. Foreman, S.M. Li, L. Tan, S. Adenwalla, A. Gruverman, S. Ducharme, Ferroelectric polymer nanopillar arrays on flexible substrates by reverse nanoimprint lithography, J. Mater. Chem. C 4 (25) (2016) 5914–5921.
[13] V. Bhavanasi, D.Y. Kusuma, P.S. Lee, Polarization orientation, piezoelectricity, and energy harvesting performance of ferroelectric PVDF-TrFE nanotubes synthesized by nanoconfinement, Adv. Energy Mater. 4 (16) (2014).
[14] Piezoelectricity: Evolution and Future of a Technology, edited by Walter Heywang, Karl Lubitz, Wolfram Wersing, Publisher: Springer-Verlag Berlin Heidelberg.
[15] L.X. Ruan, X.N. Yao, Y.F. Chang, L.Q. Zhou, G.W. Qin, X.M. Zhang, Properties and applications of the beta phase poly(vinylidene fluoride), Polymers 10 (3) (2018).
[16] P. Sharma, D. Wu, S. Poddar, T.J. Reece, S. Ducharme, A. Gruverman, Orientational imaging in polar polymers by piezoresponse force microscopy, J. Appl. Phys. 110 (5) (2011), 052010.
[17] Z. Xiao, J. Song, D.K. Ferry, S. Ducharme, X. Hong, Ferroelectric-domain-patterning-controlled Schottky junction state in monolayer ${\mathrm{MoS}}_{2, Phys. Rev. Lett. 118 (23) (2017), 236801.
[18] A. Dazzi, C.B. Prater, AFM-IR: technology and applications in nanoscale infrared spectroscopy and chemical imaging, Chem. Rev. 117 (7) (2017) 5146–5173.
[19] A.M. Katzenmeyer, V. Aksyuk, A. Centrone, Nanoscale infrared spectroscopy: improving the spectral range of the photothermal induced resonance technique, Anal. Chem. 85 (4) (2013) 1972–1979.
[20] A. Centrone, Infrared imaging and spectroscopy beyond the diffraction limit, in: R. G. Cooks, J.E. Pemberton (Eds.), Annual Review of Analytical Chemistry, Vol 8 vol. 8, 2015, pp. 101–126. Annual Reviews: Palo Alto.
[21] A. Dazzi, F. Glotin, R. Carminati, Theory of infrared nanospectroscopy by photothermal induced resonance, J. Appl. Phys. 107 (12) (2010), 124519.
[22] L.Y. Kong, J.J. Stapleton, G.R. Ziegler, Characterization of macromolecular orientation in kappa-carrageenan fibers using polarized Fourier-transform infrared spectroscopy, Vib. Spectrosc. 94 (2018) 61–65.
[23] N. Shioya, T. Shimoaka, R. Murdey, T. Hasegawa, Accurate molecular orientation analysis using infrared p-polarized multiple-angle incidence resolution spectrometry (pMAIRS) considering the refractive index of the thin film sample, Appl. Spectrosc. 71 (6) (2017) 1242–1248.
[24] P.A. Yuya, D.C. Hurley, J.A. Turner, Contact-resonance atomic force microscopy for viscoelasticity, J. Appl. Phys. 104 (7) (2008).
[25] J.P. Killgore, F.W. DelRio, Contact resonance force microscopy for viscoelastic property measurements: from fundamentals to state-of-the-art applications, Macromolecules 51 (18) (2018) 6977–6996.
[26] J.P. Killgore, D.G. Yablon, A.H. Tsou, A. Gannepalli, P.A. Yuya, J.A. Turner, R. Proksch, D.C. Hurley, Viscoelastic property mapping with contact resonance force microscopy, Langmuir 27 (23) (2011) 13983–13987.
[27] D.C. Hurley, S.E. Campbell, J.P. Killgore, L.M. Cox, Y.F. Ding, Measurement of viscoelastic loss tangent with contact resonance modes of atomic force microscopy, Macromolecules 46 (23) (2013) 9396–9402.
[28] R.F. Ding, C.W. Yang, K.Y. Huang, I.S. Hwang, High-sensitivity imaging with lateral resonance mode atomic force microscopy, Nanoscale 8 (43) (2016) 18421–18427.
[29] M. Satthiyaraju, T. Ramesh, Effect of annealing treatment on PVDF nanofibers for mechanical energy harvesting applications, Mater. Res. Express 6 (10) (2019), 105366.
[30] S. Kaur, A. Kumar, A.L. Sharma, D.P. Singh, Influence of annealing on dielectric and polarization behavior of PVDF thick films, J. Mater. Sci. Mater. Electron. 28 (12) (2017) 8391–8396.
[31] M. Baniasadi, Z. Xu, J. Cai, S. Daryadel, M. Quevedo-Lopez, M. Naraghi, M. Minary-Jolandan, Correlation of annealing temperature, morphology, and electro-mechanical properties of electrospun piezoelectric nanofibers, Polymer 127 (2017) 192–202.
[32] A. Dazzi, C.B. Prater, Q.C. Hu, D.B. Chase, J.F. Rabolt, C. Marcott, AFM-IR: combining atomic force microscopy and infrared spectroscopy for nanoscale chemical characterization, Appl. Spectrosc. 66 (12) (2012) 1365–1384.
[33] M. Kobayashi, K. Tashiro, H. Tadokoro, Molecular vibrations of three crystal forms of poly(vinylidene fluoride), Macromolecules 8 (2) (1975) 158–171.
[34] W. Qian, S. Sun, J. Song, C. Nguyen, S. Ducharme, J.A. Turner, Focused electron-beam- induced deposition for fabrication of highly durable and sensitive metallic AFM-IR probes, Nanotechnology 29 (33) (2018), 335702.
[35] G.A. Voyiatzis, K.S. Andrikopoulos, G.N. Papatheodorou, E.I. Kamitsos, G. D. Chryssikos, J.A. Kapoutsis, S.H. Anastasiadis, G. Fytas, Polarized resonance Raman and FTIR reflectance spectroscopic investigation of the molecular orientation in industrial poly(vinyl chloride) specimens, Macromolecules 33 (15) (2000) 5613–5623.
[36] F. Pirani, M. Bartolomei, V. Aquilanti, M. Scotoni, M. Vescovi, D. Ascenzi, D. Bassi, D. Cappelletti, Collisional orientation of the benzene molecular plane in supersonic seeded expansions, probed by infrared polarized laser absorption spectroscopy and by molecular beam scattering, J. Chem. Phys. 119 (1) (2003) 265–276.
[37] E. Dillon, K. Kjoller, C. Prater, Lorentz contact resonance imaging for atomic force microscopes: probing mechanical and thermal properties on the nanoscale, Microsc. Today 21 (6) (2013) 18–24.
[38] E. Rezaei, J.A. Turner, Contact resonances of U-shaped atomic force microscope cantilevers, J. Appl. Phys. 119 (2016), 034303.
[39] E. Rezaei, J.A. Turner, Contact resonance AFM to quantify the in-plane and out-of-plane loss tangent of polymers simultaneously, Appl. Phys. Lett. 110 (2017), 101902.
[40] A.B. Churnside, R.C. Tung, J.P. Killgore, Quantitative contact resonance force microscopy for viscoelastic measurement of soft materials at the solid–liquid interface, Langmuir 31 (40) (2015) 11143–11149.
[41] W. Qian, W. Li, C. Nguyen, T.J. Johnson, J.A. Turner, Quantitative nanoscale measurements of the thermomechanical properties of poly-ether-ether-ketone (PEEK), J. Polym. Sci. 58 (11) (2020) 1544–1552.